Exciton-Condensate-Like Energy Transport in Light-Harvesting Complex 2

Anna O. Schouten and David A. Mazziotti*
Department of Chemistry and The James Franck Institute, The University of Chicago, Chicago, Illinois 60637, USA

(Received 2 August 2024; revised 22 November 2024; accepted 21 January 2025; published 13 February 2025)

Bose-Einstein condensation of excitons, with its potential for frictionless energy transport, has recently been observed in materials at low temperatures. Here, we show that partial exciton condensation plays a significant role in the 18-chromophore B850 ring of the light-harvesting complex 2 (LH2) in purple bacteria. Even in the single-excitation regime, we observe that excitonic entanglement across multiple sites exhibits signatures of exciton condensation in the particle-hole reduced density matrix—a partial exciton condensate. Crucially, we find that, by distributing the exciton across multiple sites of the ring, the exciton-condensate-like state sets favorable conditions for enhanced energy transfer, both before and after decoherence. Surprisingly, this discovery reveals that excitonic condensation, previously thought to require extreme conditions, can occur in a partial form in biological systems under ambient conditions, providing new insight into energy transport. These results additionally bring new insight into the long-standing debate on quantum versus classical mechanisms in photosynthetic light harvesting by showing that quantum coherence, in the form of a partial exciton condensate, indirectly initializes subsequent classical transfer. Our findings not only deepen our understanding of quantum coherence in light harvesting but also suggest design principles for materials capable of leveraging excitonic entanglement for efficient energy transport.

DOI: 10.1103/PRXEnergy.4.013004

I. INTRODUCTION

Photosynthesis has inspired scientists for decades due to the extreme efficiency with which nature transfers energy in the form of excitons. On the other hand, exciton condensation—or the quantum condensation of excitons—promises the potential for dissipationless exciton transport, resulting in a frictionless energy flow [1]. However, the occurrence of condensation generally depends on highly ordered structures and extreme conditions such as low temperatures, high pressures, or strong magnetic fields [1–4]. The idea that nature may utilize quantum effects and phenomena for energy-transfer processes is well established [5–26] but clear connections between a macroscopic quantum phenomenon such as exciton condensation and exciton transfer in a noisy microscopic system such as a light-harvesting complex are less known. Recently, a connection between these two ideas has been found by demonstrating computationally an exciton-condensate-like state in a model of the Fenna-Matthews-Olson (FMO) complex [24], the light-harvesting complex of green sulfur bacteria. The connection between photosynthetic light harvesting and localized exciton condensation is significant because it represents the potential for synthetically realizing a local microscopic type of condensation that may retain some of the beneficial properties of macroscopic condensation even in noisy conditions at room temperature.

In this study, we explore the phenomenon of partial exciton condensation in the B850 ring of light-harvesting complex 2 (LH2) of purple bacteria, focusing on its statistical correlation with energy transfer to an energy reservoir. Partial exciton condensation refers to a quantum phase in which one or more excitons become entangled across multiple chromophores, forming a coherent state that exhibits occupation of multiple excitons in a quantum state. Importantly, because of quantum entanglement, we show that partial exciton condensation is possible even in the single-excitation regime. Our results demonstrate that the formation of this partial condensate in LH2 significantly correlates with enhanced exciton-transfer efficiency. By distributing the exciton across multiple sites within the chromophore ring, the condensate sets favorable initial conditions for efficient energy transport, ultimately improving the transfer to an energy reservoir.

Crucially, we find that the formation of partial exciton condensates initializes the state of the B850 ring for the subsequent primarily classical energy transfer. While the

*Contact author: damazz@uchicago.edu

condensate eventually decoheres, it plays a pivotal role in optimizing the energy distribution of the system, preparing the system for transfer of excitons through classical mechanisms such as hopping. This dual-stage process, where quantum coherence in the form of a partial exciton condensate initializes the system for classical transfer, provides new insight into the long-standing debate regarding the interplay between quantum and classical mechanisms in photosynthetic light harvesting [10,27,28]. Our findings suggest that quantum coherence, even if transient, has a profound impact on a second phase of more-classical energy transport.

Partial exciton condensation has recently been observed by the authors in the Fenna-Matthews-Olson (FMO) complex [24]. In that work, we have focused on a three-chromophore subset, representing each chromophore with a correlated multielectron model. This approach has allowed us to examine partial condensation arising not only from the entanglement between chromophores but also from the correlation of the electrons within the π system of each chromophore. In the present study, we examine the larger 18-chromophore ring of LH2, enabling us to explore the possibility of partial exciton condensation in a light-harvesting complex much closer in structure to those found in plants. Unlike the energy gradient-driven FMO complex, LH2 consists of nearly degenerate chromophores [17]. Our results suggest a universality of partial exciton condensation across light-harvesting complexes, occurring in both FMO and LH2, and provide critical new insight into the synergistic role of quantum coherence and classical-transfer mechanisms in optimizing energy transport.

II. THEORY

The system is modeled after the B850 ring of light-harvesting complex 2 (LH2) of purple bacteria. LH2 is part of the light-harvesting network of purple bacteria and consists of B800 and B850 rings, named for the wavelength at which each absorbs [32]. Light is absorbed by the B800 ring, transferred to the B850 ring, then passed through the B850 ring to light-harvesting complex 1 (LH1), and finally transmitted to the reaction center. As shown in Fig. 1, the B800 ring consists of 8–9 weakly coupled chromophores, while the B850 has a smaller radius but twice as many chromophores arranged in face-to-face dimers, each with an α and β chromophore. Consequently, the B850 ring has much stronger coupling between chromophores. For this reason, the B850 ring is of primary interest, as it constitutes a system of approximately degenerate, strongly coupled sites known to be capable of highly efficient energy transfer. The Hamiltonian is constructed as an 18-site ring following Ref. [17] as described in the Appendix. Results are sampled for 50 manifestations of the Hamiltonian to sample the effects of static disorder. The dynamics are simulated with MAPLE [33] using the Lindblad equation; the exciton population from an initial excitation is eventually transferred to a sink representing extraction of the exciton population from B850 to the next phase of light harvesting, i.e., transfer to LH1 or other LH2 complexes. The population of the sink is used throughout as a proxy for the ability of the system to achieve sufficient delocalization to move population from one side of the ring to the other. Delocalization is important for initializing the system for further transfer after decoherence of the quantum state. Transfer is simulated for 1000 fs to allow for transition from quantum to classical exciton transfer. Additional methodological details are given in the Appendix.

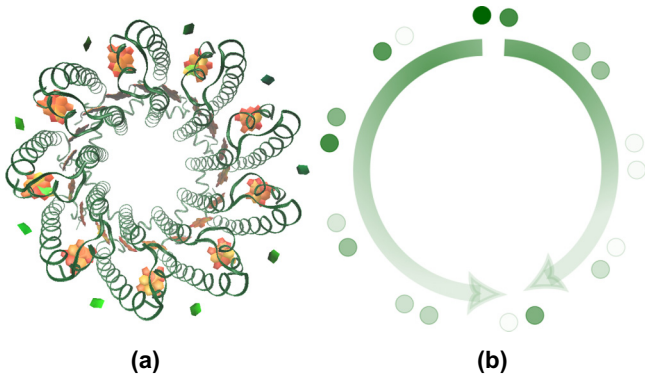

FIG. 1. (a) A top-down view of the structure of LH2 [29–31], showing the B800 (outer) and B850 (inner) rings along with the surrounding proteins. (b) A schematic view of the model of the B850 ring, with arrows demonstrating the motion of the excitons.

A. Signature of condensation

Entanglement of excitons leading to exciton condensation or an exciton-condensate-like state is manifest as off-diagonal long-range order in the particle-hole reduced density matrix (RDM)

$$^2G^{i,j}_{k,l} = \langle\Psi|\hat{a}^\dagger_i\hat{a}_j\hat{a}^\dagger_l\hat{a}_k|\Psi\rangle. \quad (1)$$

The eigenvalues of fermion density matrices, except for those corresponding to a ground-state-to-ground-state transition, are bound by one in a noninteracting system. However, the entanglement of excitons leads to off-diagonal long-range order, the computational signature of which is a large eigenvalue (greater than one) in the particle-hole RDM corresponding to more than one exciton occupying a single particle-hole wave function [34,35]. The magnitude of the large eigenvalue indicates the occupation of the particle-hole wave function, i.e., multiple excitons occupying a single state, which is analogous to the large-eigenvalue signature of Bose-Einstein condensation (BEC) in the one-boson RDM described by Penrose and Onsager [36]. In the particle-hole RDM of an exciton-condensate

state, there are generally two large eigenvalues, only one of which corresponds to the exciton condensate. The other large eigenvalue, occurring for nearly every state, corresponds to a ground-state-to-ground-state transition with no relation to exciton condensation. This extraneous eigenvalue can be removed by creating a modified particle-hole RDM:

$$ {}^2\tilde{G}^{i,j}_{k,l} = {}^2G^{i,j}_{k,l} - {}^1D^i_j\,{}^1D^l_k, \tag{2}$$

with ${}^1D$ representing the one-particle RDM.

The density matrix of the LH2 model can be written in the exciton basis as

$$D^s_t = \langle\Psi|\hat{\sigma}^\dagger_s\hat{\sigma}_t|\Psi\rangle, \tag{3}$$

where $\hat{\sigma}^\dagger_s(\hat{\sigma}_s)$ creates (destroys) an exciton at site s. In this basis, each site consists of a single level that is either occupied or unoccupied by an exciton. The density matrix is an $(M+1)\times(M+1)$ matrix, where M is the number of sites in the ring and the "+1" represents the sink. Each site in the matrix represents one site, where the diagonal elements take values between 0 and 1 and the trace sums to 1, with the magnitude of the diagonal element indicating the occupation of that site. Off-diagonal elements represent coherences between pairs of sites. For this case, the model is in the single-excitation manifold, meaning that there is only one exciton in the density matrix. This is a reasonable approximation of photosynthesis due to the infrequency of excitation events. Following Ref. [24], the single-particle excitation block of the modified particle-hole RDM is obtained by transforming the exciton density matrix to the electron (fermion) basis, consisting of two-level sites where for each site the electron is in either the upper or the lower level. The transformation is performed using the following relations:

$$\hat{a}^\dagger_{s,+1}\hat{a}_{s,-1} = \hat{\sigma}^\dagger_s, \tag{4}$$

$$\hat{a}^\dagger_{s,-1}\hat{a}_{s,+1} = \hat{\sigma}_s, \tag{5}$$

where $\hat{a}^\dagger_{s,+1}(\hat{a}_{s,-1})$ creates (destroys) an electron in the upper (lower) level of site s. The density matrix becomes

$$\tilde{G}_{s,t} = \langle\Psi|\hat{a}^\dagger_{s,+1}\hat{a}_{s,-1}\hat{a}^\dagger_{t,-1}\hat{a}_{t,+1}|\Psi\rangle. \tag{6}$$

Importantly, there is only one other relevant sub-block of the particle-hole RDM for single-particle excitations:

$$\tilde{G}^*_{s,t} = \langle\Psi|\hat{a}^\dagger_{s,-1}\hat{a}_{s,+1}\hat{a}^\dagger_{t+1}\hat{a}_{t-1}|\Psi\rangle. \tag{7}$$

The diagonal elements of $\tilde{G}$ and $\tilde{G}^*$ are related by $\tilde{G}^*_{i,i} = 1 - \tilde{G}_{i,i}$ and the off-diagonal couplings of the two matrices are equivalent. The sub-blocks of ${}^2\tilde{G}$ are flattened from tensors to matrices. In the case of single-particle excitations, the long-range order associated with exciton condensation is entirely obtained from $\tilde{G}^*$, so an eigenvalue greater than one in this sub-block, denoted λ_G in this work, is the signature of an exciton-condensate-like state.

The significance of the λ_G signature is the correspondence with off-diagonal long-range order associated with potential for condensation and superfluidity, in analogy to large-eigenvalue signatures of off-diagonal long-range order for BEC [36] and Cooper-pair condensation [37,38]. Thus, while all excitonic entanglement leading to off-diagonal long-range order is coherence, not all excitonic coherence is off-diagonal long-range order. Differentiating between specific types of excitonic coherence can be important for elucidating features and informing experimental investigation of coherence. Within the single-excitation regime modeled for the light-harvesting complex, is it specifically the entanglement of excitons across a network of chromophores, each with an electron in a two-level system capable of forming an exciton, that leads to off-diagonal long-range order. In this instance, the signature does not signify macroscopic exciton condensation but does signify a limited microscopic type of the same off-diagonal long-range order that could have parallel properties with entanglement that results in exciton condensation in macroscopic materials.

B. *W* state

The nature of light-harvesting complexes inspires connections to quantum information and computing through the qubit-like two-state structure of chromophores and exciton-transfer processes that parallel transfer of information [25,39–41]. Comparisons to states and entanglement measures used in quantum information and computing are therefore natural for characterizing this system. In quantum information, the W state [42], which is written as

$$|\Psi\rangle = \frac{1}{\sqrt{N}}(|100\cdots0\rangle + |010\cdots0\rangle + \cdots + |000\cdots1\rangle), \tag{8}$$

represents maximal entanglement of a single excitation over any number of qubits $N \geq 3$. Because this state represents the maximal entanglement of single excitations, it represents the maximum entanglement that is observable in our model. The W state also has the property that removal of a single qubit from the state does not result in the breakdown of the entanglement between the other qubits in the state. For exciton transfer, this is important because the sites involved in transfer and the degree of entanglement of those sites changes over time. The large eigenvalue of the modified particle-hole RDM, λ_G, for the W state of N

qubits, takes the value [24]

$$\lambda_G = 2 - \frac{2}{N}. \tag{9}$$

Importantly, this places an upper bound on λ_G for any possible number of chromophores N in the light-harvesting model. Moreover, the wave function of the W state represents the delocalization character expected for a maximally entangled set of chromophores, so we can quantify the entanglement extent of other states by comparing them to the W state. In this sense, λ_G is conceptually related to the multipartite entanglement used to describe the exciton delocalization length in Ref. [25].

III. RESULTS

A. Evolution of λ_G and exciton population

Several possibilities exist for the initial excitation state of the system. We choose two different excitations: an incoherent excitation (spatially localized with a single site excited) and a coherent excitation (energetically localized excitation determined by diagonalization of the Hamiltonian). Note that for both excitations, there are N possible excitation states, where N is the number of sites. For the spatial excitation, we arbitrarily select one site for excitation and designate this site 1; this type of incoherent excitation is most consistent with natural photoexcitation from sunlight or incoherent hopping from the B800 ring. In the energetic excitation, the initial excitation is selected based on the greatest contribution to the λ_G mode from the spatially excited results (for details, see the Appendix) to maximize the character of that mode. This type of energetic localization is sometimes referred to as the "exciton" representation and is associated with the excitation expected from coherent optical excitation of the system [39]. The upper limit of an entangled delocalized state in this case would be a W state, consisting of a maximally entangled state of all N sites that has the highest possible

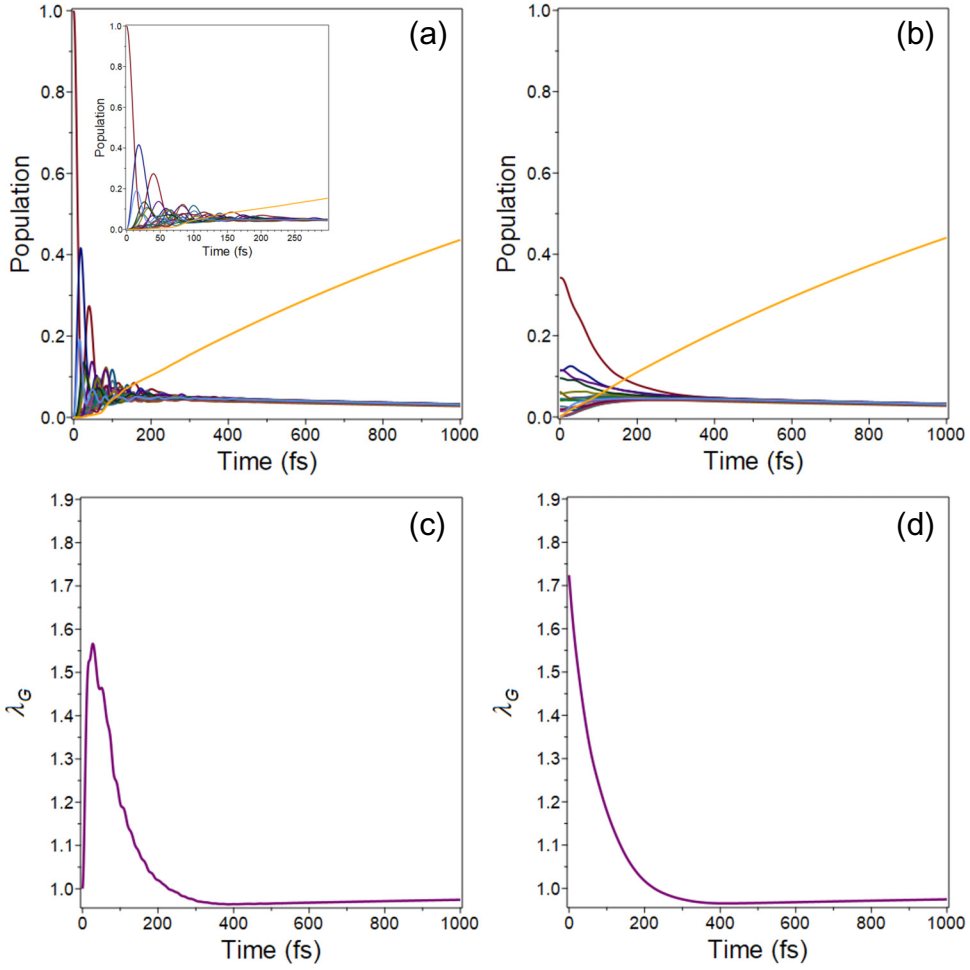

FIG. 2. (a),(b) The population dynamics of the simulations with (a) spatially localized and (b) energetically localized excitations. Each color corresponds to a different chromophore site, with the burgundy line representing site 1 and the bright yellow line the population transferred to the sink. (c),(d) The λ_G dynamics of the simulation with (c) spatially localized and (d) energetically localized excitations.

TABLE I. The maximum values of λ_G and final occupation of the sink after 1000 fs for the spatially localized and energetically localized excitation models.

	Initial excitation models	
	Spatial	Energetic
λ_G	1.58 ± 0.028	1.69 ± 0.131
Sink	0.3984 ± 0.03996	0.3950 ± 0.03434

value of λ_G in the initial state. In our system, a W state is a density matrix with all sites sharing equal population of $1/N$, coupled equally together with coupling values of $1/N$.

The results of the population and λ_G dynamics for a representative Hamiltonian with both excitation models are shown in Fig. 2. At long timescales (by approximately 500 fs), both excitation models reach equilibrium with approximately equal populations in all 18 sites, although due to static disorder in the site energies, the site populations are not precisely equal (for details, see the Appendix) [43]. By this point, exciton transfer has moved into the classical regime of incoherent transfer [44,45]. Because we are interested in the impact of the coherent state on the system, the simulations are run for 1000 fs and the remaining classical-transfer regime is ignored. The final populations of the sink (see Table I) after 1000 fs for each excitation condition are similar, demonstrating that the transfer efficiency is invariant to the excitation regime for this model. Additionally, with the spatial-excitation model, after the initial time step the population oscillates between sites prior to reaching equilibrium. In contrast, with the energetic excitation, the population decays or increases smoothly to bring the site populations to equilibrium. This is not unexpected, as the energetic excitation is an eigenstate of the Hamiltonian associated with coherent excitation, while the spatial excitation is associated with incoherent excitation with respect to the Hamiltonian. In each case, the value of λ_G reaches a peak larger than 1 and then decays to below 1 between 300 and 400 fs, prior to exciton transfer moving into the classical regime. With energetic excitation, the maximum value of λ_G is at the initial time step, implying that the eigenstates of the Hamiltonian are significantly entangled states, particularly since the value of λ_G approaches so close to the upper bound set by the W state. Indeed, analysis of the density matrices constructed from the eigenstates of the Hamiltonian indicates that all eigenstates exhibit large λ_G, just with varying magnitude (see the Appendix).

B. Correlation between λ_G and exciton transfer

To probe the relationship between λ_G and exciton transfer, we adjust the intersite coupling of the Hamiltonian to observe the influence on each quantity and report averages and standard deviations for 50 manifestations of the Hamiltonian. For the spatial excitation, in Fig. 3 we show a plot of the maximum λ_G versus the sink population where intersite coupling of the Hamiltonian is scaled by values of 0.25–3.0. Reducing coupling reduces both the maximum λ_G and the total population transferred to the sink, although there is a threshold for increasing the coupling after which neither λ_G nor the sink population increases significantly. The plot shows a strong relationship between the two quantities, which are fitted to a $1/x$ fit with $R^2 = 0.9914$. In addition to the trend with respect to the maximum λ_G and the sink population, there is an interesting trend with respect to the standard deviations of the maximum λ_G. As the degree of coupling in the Hamiltonian increases, the standard deviations decrease, as seen in Fig. 3. This behavior corresponds with how closely λ_G approaches the upper bound of maximal entanglement; tighter coupling leads to greater entanglement, which reduces the potential variability in λ_G.

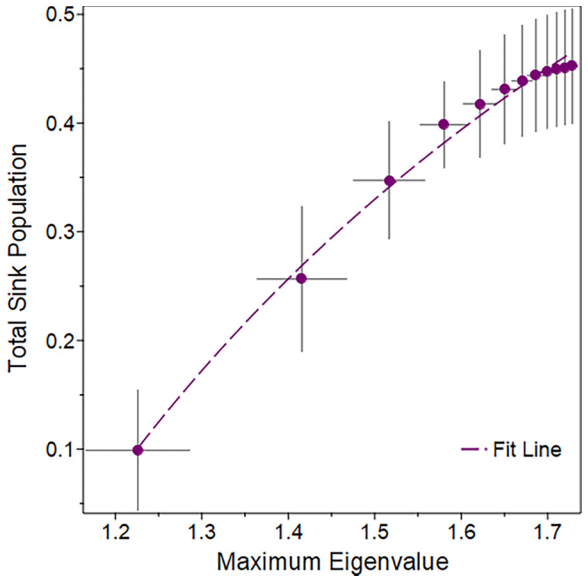

FIG. 3. A plot of the average maximum λ_G versus the sink population after 1000 fs for the spatial excitation, with Hamiltonian coupling scaled from 0.25 to 3.0. The dashed line is a $1/x$ fit: $y = 1.355 - 1.537/x$. The bars represent standard deviations in λ_G and the sink population.

For the energetic excitation, the same data are displayed in Table II; however, the effect of coupling on both λ_G and the sink population is weaker, leading to large standard deviations, particularly for low coupling values. This is revealing because the maximum eigenvalue occurs at the initial excitation and is chosen specifically as the eigenstate of the Hamiltonian with the optimal contribution to the λ_G mode. Choosing an excitation to optimize the relationship with the λ_G mode results in variation in the degree of entanglement and delocalization in the initial state, leading to variability in the sink population. This effect could potentially be reduced by instead selecting the initial states

TABLE II. The maximum λ_G and total sink population for Hamiltonian coupling scaled from 0.25 to 3.0 with the energetic excitation selected for the initial excitation.

Coupling	λ_G	Sink
0.25	1.48 ± 0.1481	0.234 ± 0.1966
0.5	1.60 ± 0.1366	0.323 ± 0.1310
0.75	1.65 ± 0.1235	0.368 ± 0.0728
1	1.69 ± 0.1310	0.395 ± 0.0343
1.25	1.73 ± 0.0742	0.420 ± 0.0244
1.5	1.76 ± 0.0547	0.432 ± 0.0207
1.75	1.77 ± 0.0441	0.432 ± 0.0170
2	1.79 ± 0.0350	0.441 ± 0.0160
2.25	1.79 ± 0.0441	0.444 ± 0.0175
2.5	1.80 ± 0.0298	0.442 ± 0.0125
2.75	1.80 ± 0.0296	0.444 ± 0.0125
3	1.80 ± 0.0275	0.450 ± 0.0156

for each of the 50 Hamiltonians to have similar values of λ_G rather than selecting for the relationship to the λ_G mode of the spatially excited simulation.

Although the relationship between λ_G and the sink population may appear trivial, indicating merely that both are correlated with the degree of coupling, the results help to highlight an important feature of the relationship. The value of λ_G indicates the formation of a highly entangled delocalized state upon or soon after initial excitation. This is significant because the key factor necessary for efficient transfer from one location in the ring to the opposite side, as in the model, is delocalization. In the case of this system, the correlation between the sink population and λ_G shows that the delocalization enabling transfer from one side of the ring to the other—for which the population of the sink is an indicator—cannot be achieved without also forming a highly entangled state exhibiting large λ_G. Likewise, factors that eliminate or reduce the entangled state also mean that delocalization allowing for transfer to the state does not occur effectively.

C. Delocalization of the λ_G state

To understand the nature of the exciton-condensate-like state, we examine the populations of the sites within the eigenstate of λ_G, V_{site} (for details, see the Appendix). V_{site} signifies the site populations of the complex only within the specific eigenstate associated with the large λ_G, calculated as the diagonal elements of the density matrix formed from the eigenvector of λ_G, $\rho_{\lambda_G} = |v_G\rangle\langle v_G|$. Because of the transformation from $\tilde{G}$ to $\tilde{G}^*$, the values of V_{site} are inversely related to the exciton populations. In Fig. 4, we show the population distributions of V_{site} at maximum λ_G for each excitation condition. The distributions show sites in ascending order, although site 1 is adjacent to both site 2 and site 18 and site 9 is spatially farthest from site 1 because of the circular shape of the system. The dotted line shows an equal eigenvector population of 1/18 in all 18 sites (site 19 is the sink) for the W state, representing the ideal entanglement of 18 sites. Equal eigenvector populations in a W state represent a distinctly different type of state than that of the system at which the populations of the density matrix reach equilibrium. This is partly because equal populations in the density matrix do not necessarily imply equal populations in the eigenvector (see below for more details) but also because the equilibrium of density-matrix populations at long timescales occurs in conjunction with the loss of off-diagonal coherence.

For the spatial excitation, the maximum λ_G occurs early in the simulation, ranging from 19 to 34 fs over the 50

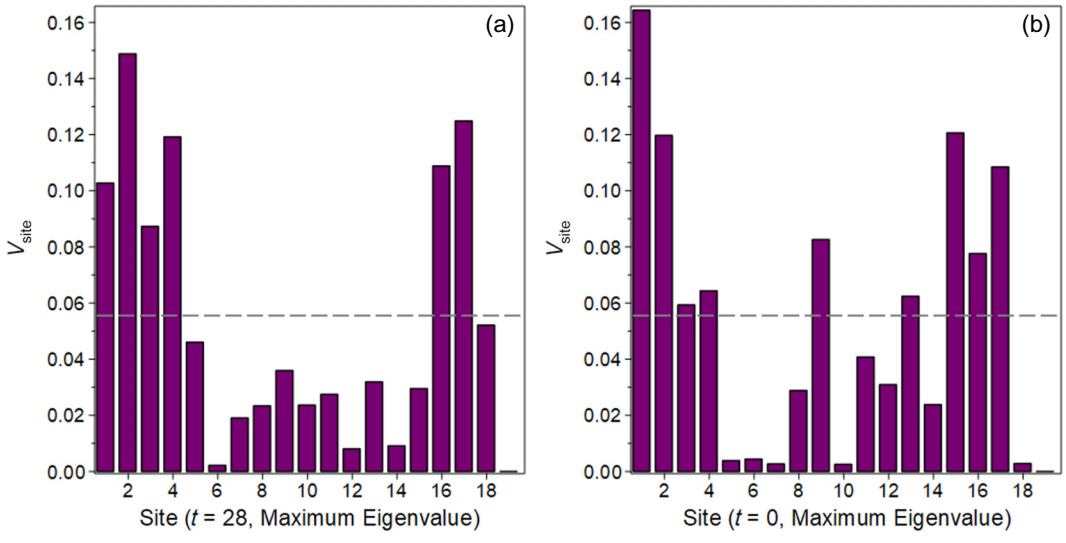

FIG. 4. The distributions of the populations of the eigenstate for maximum λ_G for the (a) spatial and (b) energetic excitation models. The dotted line represents the eigenstate populations for a maximally entangled W state.

Hamiltonians. The distribution of V_{site} is therefore still partially centered around the initial excitation site. However, some delocalization around the ring occurs, with all sites containing some population, demonstrating movement toward a highly delocalized entangled state even from a localized unentangled initial state. This occurs as the time evolution moves the system toward an eigenstate of the Hamiltonian; since eigenstates of the Hamiltonian form delocalized entangled states, the system naturally moves toward a highly entangled state. After the initial condition, the system cannot achieve a true W state due to the inclusion of the sink, which receives exciton population but is coupled to the remainder of the sites only through the Lindblad operator. Like the spatial excitation, the maximum eigenvalue of the energetic excitation is delocalized but does not form a true W state, although the magnitude of λ_G ($\lambda_G = 1.69$ with a standard deviation of 0.1310) indicates significant entanglement. Given the upper bound on λ_G ($\lambda_G = 1.8\overline{8}$), this indicates that the populated sites are significantly entangled, resembling a state close to a W state but just with fewer entangled sites. However, both the spatial and energetic excitations trend toward delocalization over all sites rather than forming maximally entangled states over only one region (e.g., population on only sites directly adjacent to sites near the excitation), suggesting that the system is seeking a state of maximum coherence over all possible sites. Nonetheless, disorder inherent in the system and loss of exciton population to the sink prevents favoring a true W state.

Plots of V_{site} over time are shown in Figs. 5(a) and 5(d) for spatial and energetic excitations. Like the density-matrix populations, the V_{site} populations display oscillatory behavior for the spatial excitation but not the energetic excitation. The V_{site} populations are delocalized until approximately 650–700 fs, after which the eigenstate becomes localized to only two sites. This is consistent with experimentally measured exciton delocalization lengths of 4 ± 2 chromophores [46]. Interestingly, localization to two sites occurs 300–400 fs after decay of λ_G to less than one, corresponding instead to the point at which all eigenvalues of $\tilde{G}^*$ begin to converge, although λ_G remains the largest eigenvalue. This point is the true

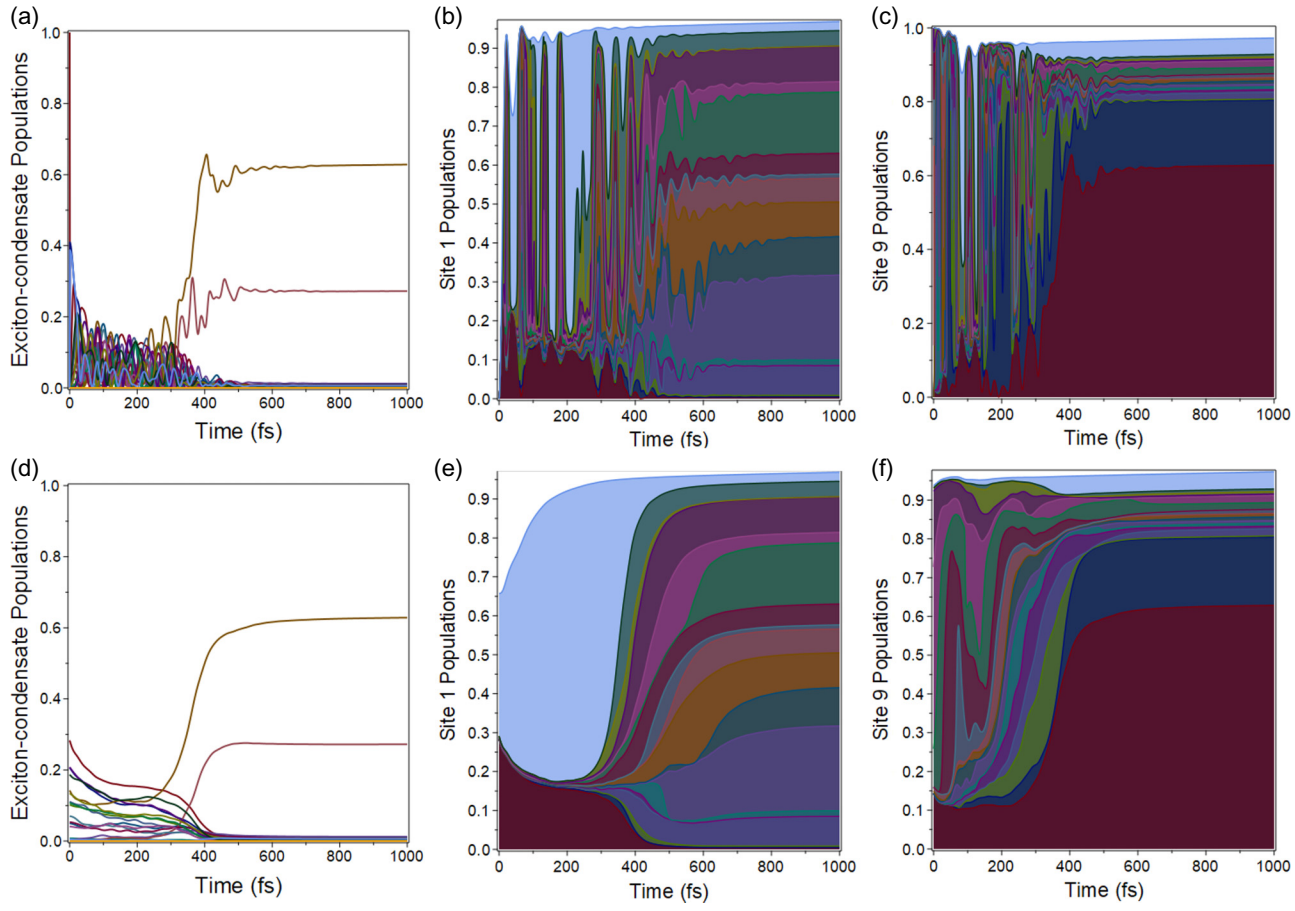

FIG. 5. The populations of the sites from the λ_G mode of the (a) spatial and (d) energetic excitation models. Each color corresponds to a site; the sink is yellow and the brown and pale red lines are sites 9 and 10, respectively. The sum of the modes of $\tilde{G}^*$ as a function of time for the (b),(c) spatial and (e),(f) energetic models for (b),(e) site 1 and (c),(f) site 9. The lowest (maroon) level corresponds to the λ_G mode of $\tilde{G}^*$ and each successive layer adds in the next-largest eigenstate.

classical transition, after which quantum coherence is lost and exciton transfer occurs classically. The sites at which V_{site} becomes localized are the sink-transfer anchor and the adjacent β site and, hence, the V_{site} populations remain trapped in the sites at which the greatest exciton transfer occurs in the classical regime. This has implications for the classical-transfer regime, indicating that the λ_G eigenstate is setting up the system for classical transfer by delocalizing population to the sites adjacent to the sink, to enable transfer by hopping. In the absence of a sink, localization occurs later (for details, see the Appendix), around 900 fs, meaning that inclusion of the transfer site causes the system to lose coherence more quickly. Additionally, in the absence of a sink, the V_{site} populations instead localize to the lowest-energy sites.

We consider the uniqueness and significance of the λ_G eigenstate to total exciton transfer by examining the contributions of all eigenstates of $\tilde{G}^*$ to specific site populations. In Figs. 5(b) and 5(c) and Figs. 5(e) and 5(f), we show plots of the eigenstate contributions over time for sites 1 and 9 for the spatial and energetic excitations. These sites have been selected because site 1 is the excitation site for the spatial excitation and site 9 is the sink-transfer anchor. The given site population in the eigenstate associated with λ_G is plotted in dark maroon and each successive layer in the plot adds the contribution to the site population of the next-largest eigenstate; hence, the total site population is plotted in light blue. For the site-1 population, the λ_G eigenstate has a more significant role in the total behavior prior to the decay of λ_G. However, for the site-9 population, the contribution of the λ_G eigenstate is greater near the end of the simulation, corresponding to the localization of the V_{site} to the sites adjacent to the sink anchor. Moreover, the quantum-classical transition is apparent in these plots from the onset of a significant change in the behavior of all eigenstates. The large contributions of the λ_G mode to site 9 following the quantum-classical transition suggests that the mode remains important even after loss of coherence. The λ_G eigenstate is also the only eigenstate for which the behavior is notable for both sites, i.e., while other eigenstates have large contributions to the dynamics on one site or the other, no other site has large contributions on both sites, meaning that this eigenstate helps to serve as the link for transferring population between these two sites.

D. Variation in λ_G with ring size

Both entanglement and the number of sites play a role in formation of the exciton-condensate-like state. To examine their influence, we reduce the number of sites in the ring and probe changes in behavior of the system. The average maximum λ_G for the spatial and energetic excitation are plotted for 4–18 sites in Fig. 6, along with the upper bound on λ_G determined from the W state. Note that in addition

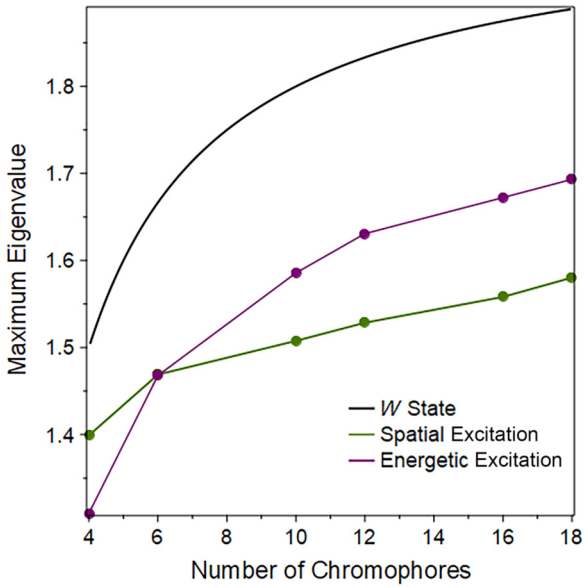

FIG. 6. The plot of the number of sites versus the average maximum eigenvalue for the spatial excitation (green) and the initial density matrix of the energetic excitation (purple). The black line shows the W-state upper bound of $2 - 2/N$, where N is the number of sites.

to reducing the number of sites, long-range coupling of the Hamiltonian is adjusted to correspond to contraction of the ring, i.e., the approximate distance between sites remains constant independent of the number of sites in the ring. The magnitude of λ_G shows little variation for the spatial excitation, decreasing only from 1.58 ± 0.0283 to 1.40 ± 0.0208 from 18 to four sites. The energetic excitation has a slightly more pronounced difference between 18 and four sites (1.69 ± 0.1310 to 1.31 ± 0.1043) but both excitation states follow the general shape of the W-state bound. It is unsurprising that the states resemble the trend of the W state, as the W state corresponds to the maximal limit of the entangled states. However, the results also reveal that for the spatial excitation, as the size of the ring contracts, the ability of the system to achieve optimal entanglement increases, as indicated by the fact that λ_G approaches nearer to the upper bound and, thus, nearer to a W state, for the ring with four sites.

IV. DISCUSSION AND CONCLUSIONS

The exciton-condensate-like state, we find, is highly correlated with exciton transfer. The correlation between these two properties demonstrates the participation of the exciton-condensate-like state in efficient exciton transfer and has implications for utilizing localized condensation to achieve highly efficient energy transport in other materials. Building upon the previous work with FMO, we clarify the role of the exciton-condensate-like state in providing entanglement leading to delocalization of excitons

that enables transfer and sets up the system for classical transfer even after decoherence of the state. In a small system such as FMO, this is less consequential, but increasing complexity and length scale, as in LH2, highlight the importance of creating conditions that allow for exciton population to efficiently move from one side of the ring to the other. Additionally, the relative lack of dependence on the initial excitation conditions in LH2 shows that, in contrast to a small system such as FMO, which is much more susceptible to differing excitation conditions, the more complex system has more inherent abilities to reach coherent states that help it achieve the most advantageous delocalized state. While the initial excitation conditions can be optimized to enhance localized condensation, the condensate state can form independent of coherence, or the lack thereof, in the initial excitation, indicating that it is a system-dependent property resulting from specific structural features rather than particular excitation conditions. Searching for other quantum systems with these features will assist in identifying materials or systems that are capable of exhibiting localized condensation. It may be that a variety of systems possess the appropriate features to be candidates for using localized condensation to initialize efficient energy transfer.

The primary requirements for formation of the exciton-condensate-like state appear to be a sufficient number of similarly coupled, relatively degenerate sites capable of forming an exciton, e.g., qubits or molecules with closely spaced highest-occupied and lowest-unoccupied orbitals, such as chlorophyll molecules in a light-harvesting complex. Unlike systems in which macroscopic exciton condensation has been observed, light-harvesting complexes are inherently noisy and not perfectly ordered. The presence of the large eigenvalue in this model shows that a perfectly ordered system—such as the model with exact degeneracy and equal coupling of sites—is not necessary for observing localized condensation. Moreover, the results demonstrate the ability of the state to maximize entanglement within the constraints of the system and utilize quantum properties even in the presence of noise and disorder. The stability of the exciton-condensate-like state to reductions in the number of sites in the ring also shows that the state can form so long as the minimum three sites are present and is only moderately enhanced by a larger number of sites due to the upper bound.

As the large eigenvalue approaches the limit of the ideal W state, this signifies the system "seeking" maximum entanglement but limited from reaching an ideal state by inherent disorder. This process of "seeking" is driven by the movement of the system toward the eigenstates of the Hamiltonian. Analysis reveals that in this case, all eigenstates of the Hamiltonian form a highly entangled exciton-condensate-like state. The disorder in the system and subsequent decoherence after time evolution place the limits on reaching a maximally entangled state. Indeed, in an otherwise equivalent but perfectly ordered system, the W state is an eigenstate of the Hamiltonian. From this analysis, an important indicator of the ability to form an exciton-condensate-like state is the presence of the large eigenvalue in eigenstates of the Hamiltonian indicating ground-state entanglement or exciton condensation. For designing new materials with the potential for exhibiting a localized exciton-condensate-like state, this could be used to verify that, in the chosen system, the exciton-forming sites are appropriately coupled to form an exciton-condensate-like state.

Examining excitonic entanglement with respect to the W state clearly underlines the relevance of the light-harvesting complex to quantum information. Light-harvesting complexes, and closely related systems, are of interest for quantum sensing and computing because they are open quantum systems capable of exchanging information with their environment; hence, the evolution of entanglement provides a quantum signal [39,41]. Understanding entanglement in this type of system, therefore, could illuminate important considerations for developing technologies and mitigating interference from environmental noise and disorder. Additional understanding may be gained by experimentally probing real systems for this effect. In light-harvesting complexes such as FMO and LH2, two-dimensional electron spectroscopy (2DES) has been used to explore coherence and exciton transport processes [47]. After excitation by coherent light, the exciton density matrix can be calculated and transformed to an appropriate basis for theoretical analysis [39]. This advanced spectroscopic approach could be applied in conjunction with the theoretical methods used in this work to probe physical systems for an exciton-condensate-like state. Recent work has also demonstrated an entanglement witness based on the cumulant of the particle-hole RDM, which also contains the large-eigenvalue signature [48], in solid-state materials from resonant inelastic x-ray scattering (RIXS) spectroscopy [49]. In materials, this could also prove to be a powerful method for identifying exciton-condensate-like states.

In a physical light-harvesting complex or synthetic material, localized exciton condensation may not necessarily be constrained by the limits of the single-excitation manifold and the W-state bound. Equilibrium ground-state exciton entanglement in a physical system may take on values that exceed the limit of a single excitation and could potentially enhance the effects of the localized condensation. The nature of the exciton-condensate-like state as a coherent state of excitons also suggests potential connections to coherent emission, i.e., superradiance [50,51], which is known to amplify energy emission and is associated with exciton delocalization in photosynthetic light-harvesting complexes [52]. Future exploration could examine possible interplay between coherent emission and localized exciton condensation in light-harvesting

complexes, providing further evidence of how nature utilizes quantum coherence for realizing function.

ACKNOWLEDGMENTS

D.A.M. gratefully acknowledges the U.S. National Science Foundation (NSF) Grant No. CHE-2155082 and the NSF "Quantum sensing for Biophysics and Bioengineering" (QuBBE) Quantum Leap Challenge Institute (NSF OMA-2121044).

APPENDIX

1. Hamiltonian

The general form of the Hamiltonian is given by

$$\hat{H} = \sum_{s,m} (\epsilon + \delta\epsilon_s)\hat{a}^\dagger_{s,m}\hat{a}_{s,m} \tag{A1}$$

$$+ \sum_{s\neq t} J_{s,t}\hat{a}^\dagger_{s,+1}\hat{a}_{s,-1}\hat{a}^\dagger_{t,-1}\hat{a}_{t,+1}, \tag{A2}$$

where s,t is the site, $m = \pm 1$ is the upper or lower level, ϵ is the site energy, $\delta\epsilon_s$ are the energy fluctuations for a specific site, and $J_{s,t}$ is the intersite coupling. The site energies, fluctuations, and coupling are defined following Ref. [17], with model parameters from Refs. [53–57]. Each site is nearly degenerate in energy, starting from degenerate energies with fluctuations added as Gaussian random noise to simulate the effects of different protein environments. The energy fluctuations are determined, following Refs. [17,54], to be a sum of Gaussian random variables with standard deviations of magnitudes $\sigma = 265$ cm^{-1} and $\sigma = 33$ cm^{-1}. The nearest-neighbor coupling includes strong coupling between the α and β sites of the same dimer ($J_{\alpha_i-\beta_i} = 320$ cm^{-1}) and weaker coupling between α and β sites of adjacent dimers ($J_{\beta_i-\alpha_j} = 250$ cm^{-1}). Long-range coupling is determined based on the dipole interactions of the sites. The B800 ring is not included in the model because the weak coupling between the B800 and B850 rings is expected to lead to incoherent excitation of the B850 ring by the B800 ring.

For the results presented in the main text, the Hamiltonian is not expanded to have multiple sites per chromophore as in Ref. [24] as the results show little difference when compared to those with only one site per chromophore. Given the nature of the LH2 Hamiltonian in comparison to that of the FMO complex, LH2 represents a nearly homogeneous system, as sites are nearly degenerate, differing in energy by random noise, and are arranged in a homogeneous pattern, while FMO is an inhomogeneous system, which has previously been shown to influence the effect of coupling on exciton transfer [58]. Additionally, the circular structure of LH2 leads to higher connectivity between sites, which, as has been demonstrated in Ref. [59], leads to increased robustness to disorder. In the expanded FMO Hamiltonian, increased or decreased exciton transfer relative to the baseline value occurs due to constructive or destructive interference between sites. A system more robust to disorder is also likely to be more robust to the effects of interference between sites, which could explain the lack of influence of the multielectron model on exciton transfer for LH2.

With respect to the exciton-condensate-like state, our conclusions regarding the requirements for state formation shed light on the differences between these two systems as well. For FMO, the magnitude of the large λ_G with a single-site excitation is independent of the number of additional chromophore sites from the multisite model and the underlying foundation for formation of the exciton-condensate-like state is the presence of multiple nearly degenerate coupled sites, just as for LH2. Consequently, the multisite model magnifies the ability of the system to demonstrate an interchromophore exciton-condensate-like state but does not inherently cause it.

TABLE III. λ_G for eigenstates of a representative Hamiltonian.

Eigenstate	λ_G
1	1.83
2	1.69
3	1.80
4	1.54
5	1.79
6	1.76
7	1.79
8	1.74
9	1.72
10	1.77
11	1.85
12	1.83
13	1.82
14	1.74
15	1.77
16	1.78
17	1.80
18	1.70

a. Hamiltonian eigenstate analysis

In Table III, we display λ_G for the density matrix constructed from the eigenstates of a representative Hamiltonian matrix.

2. Lindblad equation

Time propagation is performed using the Lindblad equation [60]:

$$\frac{d}{dt}D = -\frac{i}{\hbar}[\hat{H}, D] + \hat{L}(D), \tag{A3}$$

where $\hat{H}$ is the Hamiltonian, D is the exciton density matrix, and $\hat{L}(D)$ is the Lindblad operator. The Lindblad

operator provides dephasing and transfer of excitons to a sink,

$$\hat{L}(D) = \hat{L}_{\text{deph}}(D) + \hat{L}_{\text{sink}}(D), \tag{A4}$$

with

$$\hat{L}_{\text{deph}}(D) = \alpha \sum_k 2\langle k|D|k\rangle |k\rangle\langle k| - \{|k\rangle\langle k|, D\}, \tag{A5}$$

$$\hat{L}_{\text{sink}}(D) = \gamma \sum_\omega 2\langle \omega|D|\omega\rangle |s\rangle\langle s| - \{|\omega\rangle\langle \omega|, D\}. \tag{A6}$$

The dephasing and transfer constants are $\alpha = 0.0016$ and $\gamma = 1.451330596 \times 10^{-4}$ in atomic units. The dephasing constant is chosen to have a rate of approximately 150 fs [54,61] and the transfer rate corresponds to a transfer time of approximately 3 ps for a single sink site, in line with the experimentally predicted transfer time of 3–5 ps [32,62–65].This moves approximately 25% of the population to the sink within 500 fs. The sink is anchored to the site farthest from the initial excitation in the spatially localized framework, site 9. In a real system, excitons move from the B850 ring of LH2 to LH1 through dipole interactions, so a single site would not be expected to be "coupled" to a reaction center; instead, all sites would be expected to have some coupling to transfer population to LH1, with those nearest having a stronger coupling than those farther away. However, we find that while coupling all sites of the B850 ring to the sink—with a scaling factor determined by $1/r^3$, where r is the distance, to represent the length scale of dipole-dipole interactions—produces larger sink populations over the length of the simulation, the results are not qualitatively different from coupling a single site to the sink. We, therefore, use a single-site coupling to the sink to simplify the model and use this rate to achieve sufficient transfer to assess the role of the entangled state in exciton transfer.

3. Site populations at equilibrium

Because of static disorder in the Hamiltonian, the populations do not equilibrate to exactly equivalent values. In Fig. 7, we show populations for the spatial and energetic excitations after 500 fs for all 50 Hamiltonians to demonstrate this inequivalence. The dip in the populations represents the sink anchor site, which has lower population on average due to the draw of population to the sink. On average, the range of the site populations with the spatial excitation is 0.0152 and 0.0158 with the energetic excitation.

4. Calculation of V_{site} and energetic excitation

The energetic excitation is chosen as the eigenstate of the Hamiltonian with the largest contribution to λ_G from

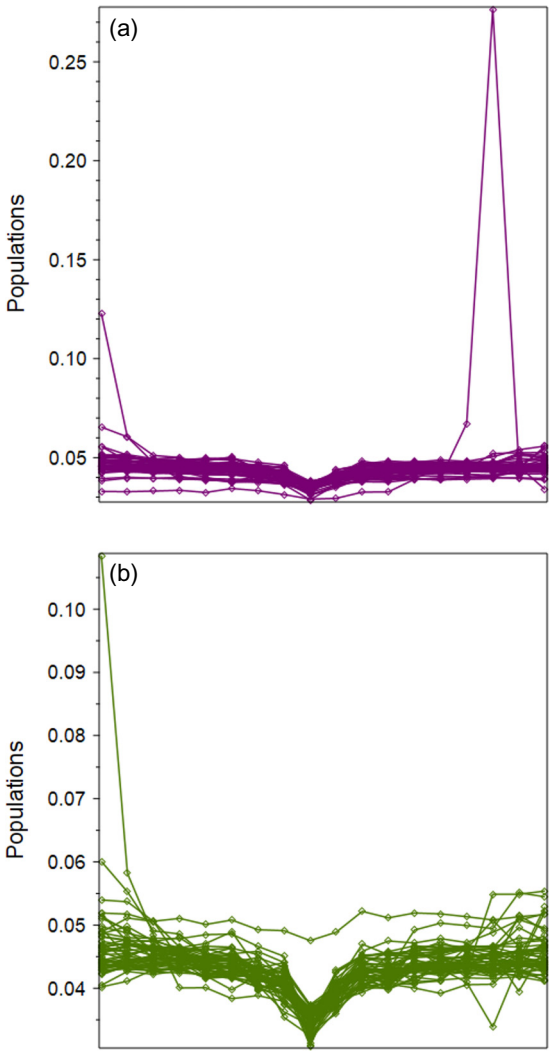

FIG. 7. The (a) spatial and (b) energetic excitation populations after 500 fs.

the spatial-excitation results. When the Hamiltonian is diagonalized as

$$\hat{H}\mu_i = \epsilon_i \mu_i, \tag{A7}$$

where the ϵ_i are the eigenvalues and the μ_i are the eigenvectors, each eigenstate represents a spatially delocalized energetically localized state. To determine which eigenstate contributes the most to λ_G, we construct a density matrix corresponding to the λ_G eigenstate from the results of the spatially localized simulation

$$\rho_{\lambda_G} = v_G \lambda_G v_G^\dagger, \tag{A8}$$

where v_G is the eigenvector of the λ_G eigenstate. The diagonals of ρ_{λ_G} correspond to the populations of the λ_G eigenvector mode, V_{site}. ρ_{λ_G} is transformed to the "exciton"

representation as

$$\rho^E_{\lambda_G} = \mu^\dagger \rho_{\lambda_G} \mu. \tag{A9}$$

The diagonal elements of $\rho^E_{\lambda_G}$ then represent the populations of the λ_G mode in the "exciton" representation, with each exciton corresponding to an eigenstate of $\hat{H}$. The eigenstate with the highest population from $\rho^E_{\lambda_G}$ has been chosen for the initial energetic excitation, i.e.,

$$D_0 = \mu_G \mu_G^\dagger. \tag{A10}$$

5. Eigenvector population dynamics with no sink

Plots of the eigenvector population dynamics with no sink are shown in Fig. 8. Note that localization occurs later in the simulation than with a sink, indicating that the quantum-classical transition occurs earlier with a sink. Additionally, rather than localizing to the sink anchor and adjacent site, the site populations V_{site} are localized to the lowest-energy sites, shown in green and sea green.

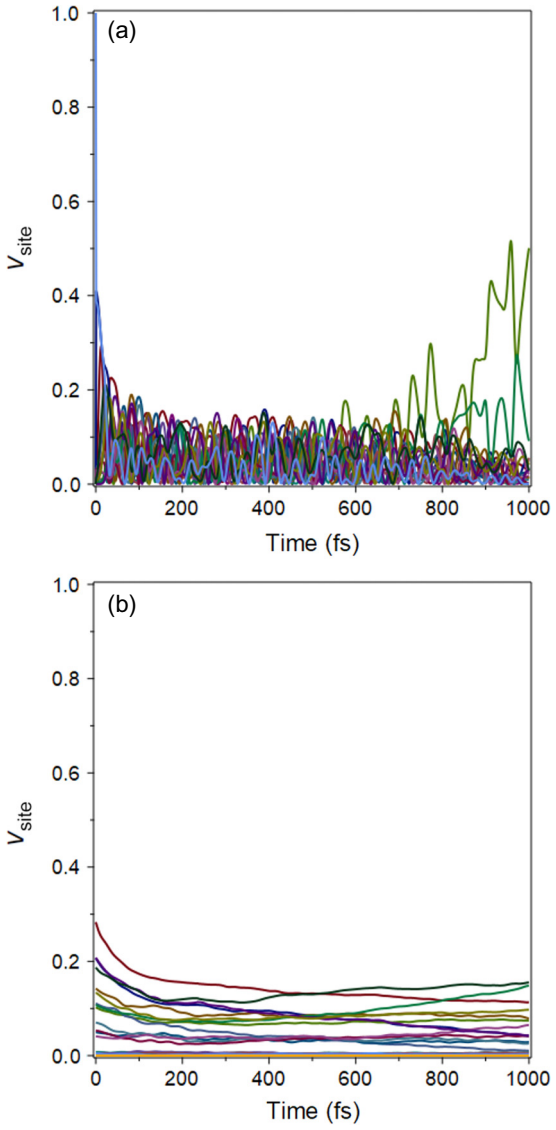

FIG. 8. Plots of the eigenvector population dynamics for the (a) spatially and (b) energetically localized excitations with no sink.

[1] L. V. Keldysh, Coherent states of excitons, Phys.-Uspekhi **60**, 1180 (2017).

[2] J. M. Blatt, K. W. Böer, and W. Brandt, Bose-Einstein condensation of excitons, Phys. Rev. **126**, 1691 (1962).

[3] H. Kalt and C. F. Klingshirn, in *Semiconductor Optics 2: Dynamics, High-Excitation Effects, and Basics of Applications* (Springer International Publishing, Cham, 2024), p. 421.

[4] P. B. Littlewood, P. R. Eastham, J. M. J. Keeling, F. M. Marchetti, B. D. Simons, and M. H. Szymanska, Models of coherent exciton condensation, J. Phys.: Condens. Matter **16**, S3597 (2004).

[5] P. Ball, Is photosynthesis quantum-ish? https://physicsworld.com/a/is-photosynthesis-quantum-ish/ physicsworld (2018).

[6] F. Caruso, A. W. Chin, A. Datta, S. F. Huelga, and M. B. Plenio, Highly efficient energy excitation transfer in light-harvesting complexes: The fundamental role of noise-assisted transport, J. Chem. Phys. **131**, 105106 (2009).

[7] S. Davidson, F. A. Pollock, and E. Gauger, Eliminating radiative losses in long-range exciton transport, PRX Quantum **3**, 020354 (2022).

[8] H.-G. Duan, V. I. Prokhorenko, R. J. Cogdell, K. Ashraf, A. L. Stevens, M. Thorwart, and R. J. D. Miller, Nature does not rely on long-lived electronic quantum coherence for photosynthetic energy transfer, PNAS **114**, 8493 (2017).

[9] R. Dutta and B. Bagchi, Delocalization and quantum entanglement in physical systems, J. Phys. Chem. Lett. **10**, 2037 (2019).

[10] G. S. Engel, T. R. Calhoun, E. L. Read, T.-K. Ahn, T. Mančal, Y.-C. Cheng, R. E. Blankenship, and G. R. Fleming, Evidence for wavelike energy transfer through quantum coherence in photosynthetic systems, Nature **446**, 782 (2007).

[11] F. Fassioli and A. Olaya-Castro, Distribution of entanglement in light-harvesting complexes and their quantum efficiency, New J. Phys. **12**, 085006 (2010).

[12] F. Fassioli, A. Olaya-Castro, and G. D. Scholes, Coherent energy transfer under incoherent light conditions, J. Phys. Chem. Lett. **3**, 3136 (2012).

[13] F. Fassioli, R. Dinshaw, P. C. Arpin, and G. D. Scholes, Photosynthetic light harvesting: Excitons and coherence, J. R. Soc., Interface **11**, 20130901 (2014).

[14] E. Z. Harush and Y. Dubi, Do photosynthetic complexes use quantum coherence to increase their efficiency? Probably not, Sci. Adv. **7**, eabc4631 (2021).

[15] Z. Hu, G. S. Engel, F. H. Alharbi, and S. Kais, Dark states and delocalization: Competing effects of quantum coherence on the efficiency of light harvesting systems, J. Chem. Phys **148**, 064304 (2018).

[16] I. Kassal, J. Yuen-Zhou, and S. Rahimi-Keshari, Does coherence enhance transport in photosynthesis? J. Phys. Chem. Lett. **4**, 362 (2013).
[17] A. Mattioni, F. Caycedo-Soler, S. F. Huelga, and M. B. Plenio, Design principles for long-range energy transfer at room temperature, Phys. Rev. X **11**, 041003 (2021).
[18] D. A. Mazziotti, Effect of strong electron correlation on the efficiency of photosynthetic light harvesting, J. Chem. Phys. **137**, 074117 (2012).
[19] M. B. Plenio and S. F. Huelga, Dephasing-assisted transport: Quantum networks and biomolecules, New J. Phys. **10**, 113019 (2008).
[20] J. E. Runeson, J. E. Lawrence, J. R. Mannouch, and J. O. Richardson, Explaining the efficiency of photosynthesis: Quantum uncertainty or classical vibrations? J. Phys. Chem. Lett. **13**, 3392 (2022).
[21] M. Saberi, M. B. Harouni, R. Roknizadeh, and H. Latifi, Energy transfer and quantum correlation dynamics in FMO light-harvesting complex, Mol. Phys. **114**, 2123 (2016).
[22] M. Sarovar, A. Ishizaki, G. R. Fleming, and K. B. Whaley, Quantum entanglement in photosynthetic light-harvesting complexes, Nat. Phys. **6**, 462 (2010).
[23] G. D. Scholes, Quantum-coherent electronic energy transfer: Did nature think of it first? J. Phys. Chem. Lett. **1**, 2 (2010).
[24] A. O. Schouten, L. M. Sager-Smith, and D. A. Mazziotti, Exciton-condensate-like amplification of energy transport in light harvesting, PRX Energy **2**, 023002 (2023).
[25] C. Smyth, D. G. Oblinsky, and G. D. Scholes, B800–B850 coherence correlates with energy transfer rates in the LH2 complex of photosynthetic purple bacteria, Phys. Chem. Chem. Phys. **17**, 30805 (2015).
[26] S. Tomasi, S. Baghbanzadeh, S. Rahimi-Keshari, and I. Kassal, Coherent and controllable enhancement of light-harvesting efficiency, Phys. Rev. A **100**, 043411 (2019).
[27] A. Ishizaki and G. R. Fleming, Theoretical examination of quantum coherence in a photosynthetic system at physiological temperature, Proc. Natl. Acad. Sci. **106**, 17255 (2009).
[28] G. D. Scholes, G. R. Fleming, L. X. Chen, A. Aspuru-Guzik, A. Buchleitner, D. F. Coker, G. S. Engel, R. van Grondelle, A. Ishizaki, D. M. Jonas, J. S. Lundeen, J. K. McCusker, S. Mukamel, J. P. Ogilvie, A. Olaya-Castro, M. A. Ratner, F. C. Spano, K. B. Whaley, and X. Zhu, Using coherence to enhance function in chemical and biophysical systems, Nature **543**, 647 (2017).
[29] M. Papiz, V. Cherezov, J. Clogston, and M. Caffrey, Structure of LH2 from *Rps. acidophila* crystallized in lipidic mesophases (2006).
[30] V. Cherezov, J. Clogston, M. Z. Papiz, and M. Caffrey, Room to move: Crystallizing membrane proteins in swollen lipidic mesophases, J. Mol. Biol. **357**, 1605 (2006).
[31] W. Humphrey, A. Dalke, and K. Schulten, VMD: Visual molecular dynamics, J. Mol. Graph. **14**, 33 (1996).
[32] R. J. Cogdell, A. Gall, and J. Köhler, The architecture and function of the light-harvesting apparatus of purple bacteria: From single molecules to *in vivo* membranes, Q. Rev. Biophys. **39**, 227 (2006).
[33] MAPLE (Maplesoft, a division of Waterloo Maple Inc., 2023).
[34] C. Garrod and M. Rosina, Particle-hole matrix: Its connection with the symmetries and collective features of the ground state, J. Math. Phys. **10**, 1855 (1969).
[35] S. Safaei and D. A. Mazziotti, Quantum signature of exciton condensation, Phys. Rev. B **98**, 045122 (2018).
[36] O. Penrose and L. Onsager, Bose-Einstein condensation and liquid helium, Phys. Rev. **104**, 576 (1956).
[37] C. N. Yang, Concept of off-diagonal long-range order and the quantum phases of liquid He and of superconductors, Rev. Mod. Phys. **34**, 694 (1962).
[38] F. Sasaki, Eigenvalues of fermion density matrices, Phys. Rev. **138**, B1338 (1965).
[39] I. Avdic, L. M. Sager-Smith, I. Ghosh, O. C. Wedig, J. S. Higgins, G. S. Engel, and D. A. Mazziotti, Quantum sensing using multiqubit quantum systems and the Pauli polytope, Phys. Rev. Res. **5**, 043097 (2023).
[40] C. Smyth and G. D. Scholes, Method of developing analytical multipartite delocalization measures for mixed *W*-like states, Phys. Rev. A **90**, 032312 (2014).
[41] Y. Zhang, C. P. Oberg, Y. Hu, H. Xu, M. Yan, G. D. Scholes, and M. Wang, Molecular and supramolecular materials: From light-harvesting to quantum information science and technology, J. Phys. Chem. Lett. **15**, 3294 (2024).
[42] W. Dür, G. Vidal, and J. I. Cirac, Three qubits can be entangled in two inequivalent ways, Phys. Rev. A **62**, 062314 (2000).
[43] J. Strümpfer and K. Schulten, Light harvesting complex II B850 excitation dynamics, J. Chem. Phys. **131**, 225101 (2009).
[44] G. D. Scholes, Long-range resonance energy transfer in molecular systems, Ann. Rev. Phys. Chem. **54**, 57 (2003).
[45] K. J. Karki, J. Chen, A. Sakurai, Q. Shi, A. T. Gardiner, O. Kühn, R. J. Cogdell, and T. Pullerits, Before Förster. Initial excitation in photosynthetic light harvesting, Chem. Sci. **10**, 7923 (2019).
[46] T. Pullerits, M. Chachisvilis, and V. Sundström, Exciton delocalization length in the B850 antenna of rhodobacter sphaeroides, J. Phys. Chem **100**, 10787 (1996).
[47] E. Fresch, F. V. A. Camargo, Q. Shen, C. C. Bellora, T. Pullerits, G. S. Engel, G. Cerullo, and E. Collini, Two-dimensional electronic spectroscopy, Nat. Rev. Methods Primers **3**, 84 (2023).
[48] A. O. Schouten, L. M. Sager-Smith, and D. A. Mazziotti, Large cumulant eigenvalue as a signature of exciton condensation, Phys. Rev. B **105**, 245151 (2022).
[49] T. Liu, L. Xu, J. Liu, and Y. Wang, Entanglement witness for indistinguishable electrons using solid-state spectroscopy, arXiv:2408.04876 [cond-mat.str-el].
[50] R. H. Dicke, Coherence in spontaneous radiation processes, Phys. Rev. **93**, 99 (1954).
[51] M. O. Scully and A. A. Svidzinsky, The super of superradiance, Science **325**, 1510 (2009).
[52] R. Monshouwer, M. Abrahamsson, F. van Mourik, and R. van Grondelle, Superradiance and exciton delocalization in bacterial photosynthetic light-harvesting systems, J. Phys. Chem. B **101**, 7241 (1997).
[53] F. Caycedo-Soler, C. A. Schroeder, C. Autenrieth, A. Pick, R. Ghosh, S. F. Huelga, and M. B. Plenio, Quantum redirection of antenna absorption to photosynthetic reaction centers, J. Phys. Chem. Lett. **8**, 6015 (2017).

[54] F. Caycedo-Soler, J. Lim, S. Oviedo-Casado, N. F. van Hulst, S. F. Huelga, and M. B. Plenio, Theory of excitonic delocalization for robust vibronic dynamics in LH2, J. Phys. Chem. Lett. **9**, 3446 (2018).

[55] T. Pullerits, S. Hess, J. L. Herek, and V. Sundström, Temperature dependence of excitation transfer in LH2 of *Rhodobacter sphaeroides*, J. Phys. Chem. B **101**, 10560 (1997).

[56] G. D. Scholes, I. R. Gould, R. J. Cogdell, and G. R. Fleming, *Ab initio* molecular orbital calculations of electronic couplings in the LH2 bacterial light-harvesting complex of *Rps. acidophila*, J. Phys. Chem. B **103**, 2543 (1999).

[57] T. Walz, S. J. Jamieson, C. M. Bowers, P. A. Bullough, and C. Hunter, Projection structures of three photosynthetic complexes from *Rhodobacter sphaeroides*: LH2 at 6 Å, LH1 and RC-LH1 at 25 Å, J. Mol. Biol. **282**, 833 (1998).

[58] C. C. Forgy and D. A. Mazziotti, Relations between environmental noise and electronic coupling for optimal exciton transfer in one- and two-dimensional homogeneous and inhomogeneous quantum systems, J. Chem. Phys. **141**, 224111 (2014).

[59] G. D. Scholes, Polaritons and excitons: Hamiltonian design for enhanced coherence, Proc. R. Soc. A **476**, 20200278 (2020).

[60] G. Lindblad, On the generators of quantum dynamical semigroups, Commun. Math. Phys. **48**, 119 (1976).

[61] A. F. Fidler, V. P. Singh, P. D. Long, P. D. Dahlberg, and G. S. Engel, Time scales of coherent dynamics in the light-harvesting complex 2 (LH2) of *Rhodobacter sphaeroides*, J. Phys. Chem. Lett. **4**, 1404 (2013).

[62] J. Linnanto and J. Korppi-Tommola, Modelling excitonic energy transfer in the photosynthetic unit of purple bacteria, Chem. Phys. **357**, 171 (2009), excited State Dynamics in Light Harvesting Materials.

[63] L. Lüer, V. Moulisová, S. Henry, D. Polli, T. H. P. Brotosudarmo, S. Hoseinkhani, D. Brida, G. Lanzani, G. Cerullo, and R. J. Cogdell, Tracking energy transfer between light harvesting complex 2 and 1 in photosynthetic membranes grown under high and low illumination, PNAS **109**, 1473 (2012).

[64] J. Ye, K. Sun, Y. Zhao, Y. Yu, C. Kong Lee, and J. Cao, Excitonic energy transfer in light-harvesting complexes in purple bacteria, J. Chem. Phys. **136**, 245104 (2012).

[65] S. Kundu, R. Dani, and N. Makri, Tight inner ring architecture and quantum motion of nuclei enable efficient energy transfer in bacterial light harvesting, Sci. Adv. **8**, eadd0023 (2022).